

pubs.acs.org/biochemistry Article

A Closed Form Model for Molecular Ratchet-Type Chemically Induced Dimerization Modules

Paul J. Steiner, Samuel D. Swift, Matthew Bedewitz, Ian Wheeldon, Sean R. Cutler, Dmitri A. Nusinow, and Timothy A. Whitehead*



Cite This: https://doi.org/10.1021/acs.biochem.2c00172

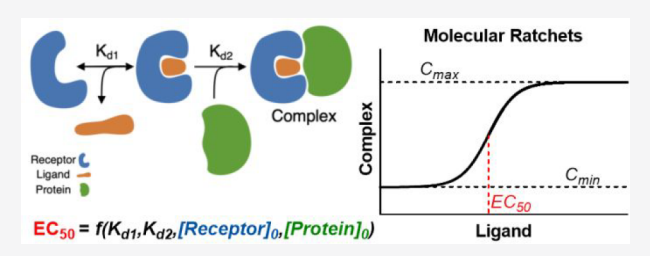


ACCESS

III Metrics & More

Article Recommendations

ABSTRACT: Chemical-induced dimerization (CID) modules enable users to implement ligand-controlled cellular and biochemical functions for a number of problems in basic and applied biology. A special class of CID modules occur naturally in plants and involve a hormone receptor that binds a hormone, triggering a conformational change in the receptor that enables recognition by a second binding protein. Two recent reports show that such hormone receptors can be engineered to sense dozens of structurally diverse compounds. As a closed form model for molecular ratchets would be of immense utility



in forward engineering of biological systems, here we have developed a closed form model for these distinct CID modules. These modules, which we call molecular ratchets, are distinct from more common CID modules called molecular glues in that they engage in saturable binding kinetics and are characterized well by a Hill equation. A defining characteristic of molecular ratchets is that the sensitivity of the response can be tuned by increasing the molar ratio of the hormone receptor to the binding protein. Thus, the same molecular ratchet can have a pico- or micromolar EC_{50} depending on the concentration of the different receptor and binding proteins. Closed form models are derived for a base elementary reaction rate model, for ligand-independent complexation of the receptor and binding protein, and for homodimerization of the hormone receptor. Useful governing equations for a variety of *in vitro* and *in vivo* applications are derived, including enzyme-linked immunosorbent assay-like microplate assays, transcriptional activation in prokaryotes and eukaryotes, and ligand-induced split protein complementation.

The discovery and exploitation of chemical-induced dimerization (CID) modules have been transformative for chemical biology and biotechnology. CID systems enable users to implement ligand-controlled cellular and biochemical functions for a number of problems in basic and applied biology. Most commonly engineered CID modules are "molecular glues" with a shared ligand binding interface.^{2,3} In these systems, the ligand can bind independently to either protein in isolation. This situation results, at high ligand concentrations, in a loss of activation as the two proteins are independently complexed with the ligand, preventing ternary complex formation. 4 Molecular glue-type CIDs occur naturally in plants for use in perception of hormones like auxin or jasmonic acid.³ In contrast to these molecular glues, CID modules with fundamentally different architecture are used by plants for the perception of the hormones abscisic acid and gibberellin.⁵ In these modules, a hormone receptor protein first binds the small molecule hormone ("ligand"), triggering a conformational change in the protein that enables recognition by a partner protein. Importantly, the partner protein cannot directly bind to the hormone by itself, thus separating hormone perception from transduction. This architecture results in saturable rather than bell-shaped kinetics. We name this second CID architecture a "molecular ratchet" because the sensitivity of hormone

occupancy can be tuned by the amount of the partner protein. Higher molar ratios of the partner protein increase the sensitivity akin to a lever effect from a ratcheting socket wrench.

Native and engineered molecular ratchets have been applied to control processes in mammalian cells, 6-8 including ligand-dependent activation of CAR-T cells. One main limitation of both molecular glues and molecular ratchets is that such modules are controlled by a relatively small palette of ligands. Park et al. originally showed that the ligand binding pocket of the *Arabidopsis thaliana* abscisic acid (ABA) receptor PYRABAC-TIN RESISTANCE 1 (PYR1) could be reprogrammed to bind four different ligands; one sensor was optimized by four rounds of directed evolution to yield a hextuple mutant with nanomolar responsiveness to mandipropamid, a nonherbicidal agrochemical in current use. Recently, Beltran et al. have shown the remarkable malleability of the PYR1 binding pocket

Special Issue: Protein Engineering

Received: March 23, 2022 Revised: May 31, 2022



by developing engineered sensors for structurally diverse compounds, including organophosphates, natural products, and synthetic cannabinoids. PYR1 and its related PYRABAC-TIN RESISTANCE-LIKE (PYL) receptors illustrate naturally occurring molecular ratchets: when these receptors bind to their natural ligand, ABA, a conformational change occurs that enables them to bind to and inhibit a subfamily of plant-type 2c protein phosphatases (PP2Cs) that include the proteins ABI1, HAB1, and other PP2Cs. We refer to these throughout as PYR1 and HAB1; however, the mechanistic details are similar for a large number of plant PYL and PP2C proteins. Receptor/ABAmediated inhibition of the PP2Cs initiates a phosphorylationmediated signal transduction cascade that activates ABA transcriptional responses and other outputs such as membrane depolarization and guard cell closure. 12 Beltran et al. 11 also showed the portability of these engineered molecular ratchets across in vivo and in vitro platforms, including development of an enzyme-linked immunosorbent assay (ELISA)-like microplate assay for sensitive ligand detection. Thus, this PYR1-based molecular ratchet platform technology has the potential to be utilized across biosensing modalities and in applications as diverse as agriculture, biocontainment, controlling cell-based therapies, and toxicology screening.

A closed form model for molecular ratchets would be of immense utility in forward engineering of biological systems. An analytical mathematical model for the binding equilibrium of ternary molecular glues has been presented.⁴ However, no corresponding closed form model for a molecular ratchet has been published, with only the set of differential equations^{3,13} and algebraic forms for limiting cases¹⁴ previously described. Therefore, in this work, we derive an analytical mathematical model for equilibrium binding for CID complexes derived from elementary rate equations. We show characteristics of the dynamics of the response, including the influence of recognition of the receptor-ligand complex by the binding protein as being key to the overall sensitivity of the system. We further show limiting cases of the model that can be used to determine underlying kinetic and equilibrium binding constants from experimental methods like enzyme inhibition assays, yeast surface display titrations, and surface plasmon resonance measurements. We show how these equilibrium constants translate to in vivo sensing modalities. Finally, we derive useful metrics for engineering systems for in vivo and in vitro applications.

MATERIALS AND EXPERIMENTAL DETAILS

Custom scripts in R, MATLAB, or Graphpad Prism were used to generate all figures presented in this work (Figures 1–5). Panels E and F of Figure 4 and panel D of Figure 5 show raw data sourced from ref 11. The remaining figures are from equations derived in this work with the indicated parameters.

RESULTS AND DISCUSSION

Mathematical Description of the Molecular Ratchet Transfer Function. Molecular glues have characteristic bell-shaped profiles where high ligand concentrations drive low rates of ternary complex formation among the receptor (R), ligand (L), and protein (P). At high ligand concentrations, the receptor and protein are saturated with the ligand and therefore no complex is formed between the two, resulting in a bell-shaped response (Figure 1A). By contrast, molecular ratchets have a saturable response, where the parameter set depends on the total

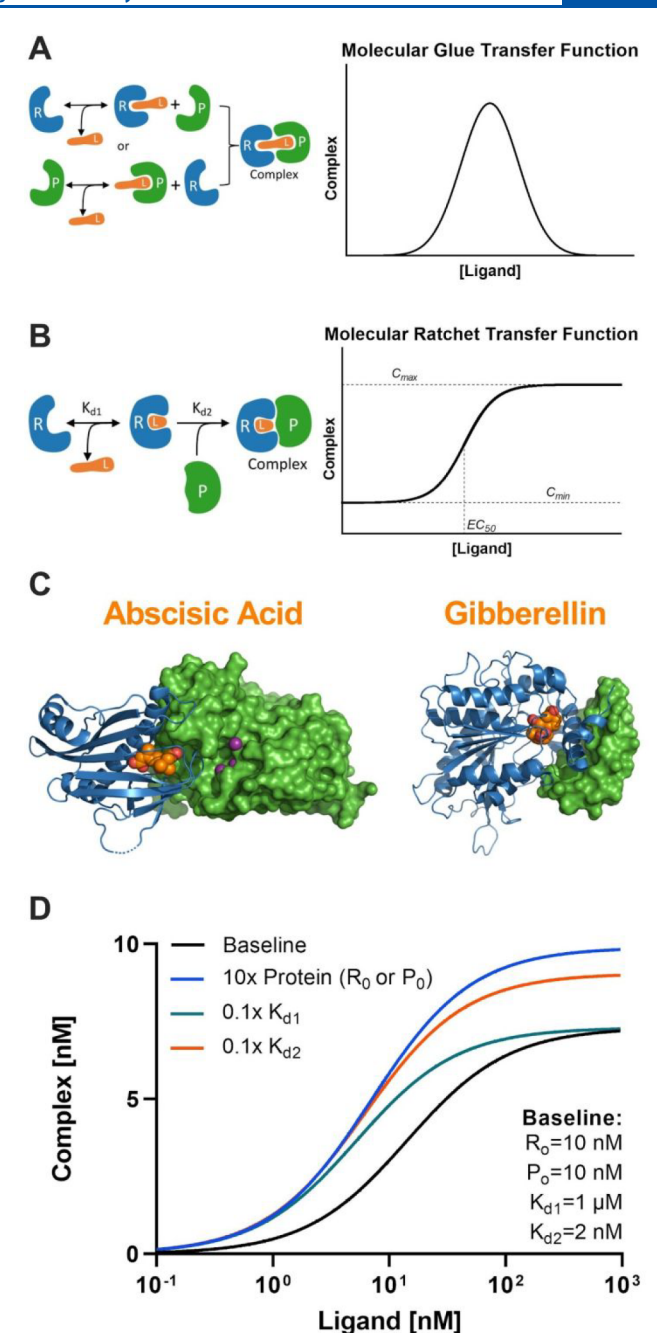


Figure 1. Overview of chemically induced dimerization (CID) modules. (A) Schematic of the molecular glue system and the corresponding bell-shaped behavior. (B) Schematic of the molecular ratchet system and the corresponding saturable transfer function. (C) Structures of natural molecular ratchets involved in plant hormone perception (PDB entries 3QN1 and 2ZSH). ^{15,16} Receptor proteins are shown as blue ribbons. Ligands are colored orange. Binding proteins are colored green. (D) Equilibrium molecular ratchet transfer function for different parameter values (P_0 , R_0 , K_{d1} , and K_{d2}).

concentrations of constituent species and the intrinsic affinities of the molecular interactions (Figure 1B). Figure 1C shows the determined structures of natural hormone perception systems in plants utilizing molecular ratchets. In this section, we derive the closed form solution for the molecular ratchet equilibrium transfer function and determine the sensitivities of the transfer function to these parameters.

Biochemistry pubs.acs.org/biochemistry Article

Consider the minimal molecular ratchet subsystem containing a protein receptor R, a ligand L, and a binding protein P. Receptor R can bind the ligand to form an R·L complex; this R·L complex can then be recognized by a binding protein P to form ternary complex C. We define the equilibrium transfer function as the dependence of complex C as a function of the concentration of ligand L. The elementary rate equations governing this minimal subsystem are as follows:

$$R + L \stackrel{K_{d1}}{\Leftrightarrow} R \cdot L$$

$$R \cdot L + P \stackrel{K_{d2}}{\Leftrightarrow} C$$

The total amounts of R, L, and P are constant, giving three conservation equations. With these constraints and the equilibrium conditions for the two reactions, we have the system of five equations that determines the steady state solution. The steady state solution is itself determined by five parameters: initial concentrations of L, R, P ([L]_o, [R]_o, and $[P]_0$, respectively), dissociation constant K_{d1} between R and L, and dissociation constant K_{d2} between the R·L complex and P. This system provides a saturable response with respect to ligand concentration. Like many biological networks, the module can be approximated by a Hill equation, where C_{\min} is the minimum concentration of complex, C_{max} the maximum concentration of complex, EC₅₀ is the effective concentration at which 50% of the maximal signal is reached. As will be shown in further detail below, this equation collapses under many realistic in vitro and in vivo conditions to the simpler three parameter equation:

$$[C] = C_{\min} + (C_{\max} - C_{\min}) \frac{[L]_{o}}{EC_{50} + [L]_{o}}$$
(1)

This Hill formalism will help us understand system behavior with respect to more familiar parameter sets for the biochemist. Figure 1D shows the molecular ratchet transfer function for a baseline set of parameters and how the perturbation of those parameters affects the system dynamics. A 10-fold increase in either protein concentration ([R]₀ or [P]₀) increases the amount of complex formed at saturation and improves the system sensitivity at lower ligand concentrations. Similarly, a 10-fold decrease in $K_{\rm d2}$, representing higher complexation affinity of the ligand-bound receptor for the protein, also results in an increased level of complex formation as well as improved sensitivity. Lastly, a 10-fold decrease in $K_{\rm d1}$ results in a somewhat improved sensitivity of the system, although the complex concentration at saturating ligand concentrations remains unaffected. Let us try to understand the system's behavior in detail.

Maximum Responsiveness. First consider the asymptotic values for [C] for low and high ligand concentrations. In the absence of a ligand, we find that C_{\min} is zero. In the limit of a very high ligand concentration, we can derive a compact expression for C_{\max} :

$$C_{\text{max}} = \frac{1}{2} \left[K_{\text{d2}} + [R]_{\text{o}} + [P]_{\text{o}} - \sqrt{(K_{\text{d2}} + [R]_{\text{o}} + [P]_{\text{o}})^2 - 4[R]_{\text{o}}[P]_{\text{o}}} \right]$$
(2)

Note that at saturating ligand concentrations the behavior of the system is a function of $[R]_o$, $[P]_o$, and K_{d2} but not K_{d1} . When R is limiting, one finds that the complex formed approaches the following expression:

$$\frac{C_{\text{max}}}{[R]_{\text{o}}} = \frac{[P]_{\text{o}}}{K_{\text{d2}} + [P]_{\text{o}}}$$
(3)

A similar expression is observed when P is limiting. We find that in many cases the maximum concentration attained is close to the value of the limiting protein (either R or P); such cases are found whenever $[P]_o \gg K_{\rm d2}$ (Figure 2A). This finding sets a strong constraint on natural or engineered systems where any free P must be completely complexed. In such cases, $[R]_o > [P]_o \gg K_{\rm d2}$, which requires low nanomolar $K_{\rm d2}$, as higher values would require medium micromolar or higher concentrations of the receptor.

Closed Form Solution for Molecular Ratchets. Now, let us understand the behavior of the sensitivity and cooperativity for molecular ratchets. No convenient closed form of the solution for complex concentration [C] can be obtained. However, a closed form solution can be written for the initial receptor concentration as a function of other parameters. By symmetry, the same expression can be written for initial ligand concentrations:

$$[L]_{o} = [C] + \frac{[C]}{[P]_{o} - [C]} K_{d2} + K_{d1} \frac{\frac{[C]}{[P]_{o} - [C]} K_{d2}}{[R]_{o} - \frac{[C]}{[P]_{o} - [C]} K_{d2} - [C]}$$
(4)

This expression allows us to understand the transfer functions plotted in Figure 1D. First, consider the strong receptor—ligand binding limit ($K_{\rm d1} \rightarrow 0$). In this limit, the solution reduces to

$$[L]_{o} = [C] + \frac{[C]}{[P]_{o} - [C]} K_{d2}$$
 (5)

This means that the maximum sensitivity of the system is controlled by $K_{\rm d2}$ no matter how small $K_{\rm d1}$ becomes. However, in the limit of $K_{\rm d2} \rightarrow 0$, the system collapses to the trivial solution $[C] = [L]_{\rm o}$ where every additional ligand molecule added to the system is taken up in the complex. This finding that sensitivity is to a large extent controlled by the affinity of the bound receptor for binding protein P, and not receptor—ligand binding affinity, is important and will be further evaluated below.

Molecular Ratchets Show Minimal Cooperativity. The closed form solution allows us to understand both the cooperativity of the response and the sensitivity. In biochemistry derivations, cooperativity is usually defined by an empirical fit of the Hill equation with the Hill coefficient defining the magnitude of cooperativity. We comprehensively sampled Hill coefficients over the biochemically relevant parameter space. Over this range, converted Hill coefficients vary only between a narrow window of 1-2, indicating a cooperative but not ultrasensitive response. The Furthermore, under most conditions where an EC is measured in vitro (either low nanomolar concentrations of P or R) or under in vivo applications, the Hill coefficient approaches 1. Thus, under most conditions, molecular ratchets observe minimal cooperativity.

Molecular Ratchet Sensitivity Is Tuned by Ratios between Proteins and K_{d2} . We define an EC₅₀ as the ligand concentration at which [C] is 50% of $C_{\rm max}$. Thus, we can solve for EC₅₀ rigorously by first solving for $C_{\rm max}$ and then solving for the ligand concentration according to the following relationship:

$$EC_{50} = \frac{1}{2}C_{\text{max}} + \frac{C_{\text{max}}}{2[P]_{\text{o}} - C_{\text{max}}} K_{\text{d2}} + K_{\text{d1}} \frac{\frac{C_{\text{max}}}{2[P]_{\text{o}} - C_{\text{max}}} K_{\text{d2}}}{[R]_{\text{o}} - \frac{C_{\text{max}}}{2[P]_{\text{o}} - C_{\text{max}}} K_{\text{d2}} - \frac{1}{2}C_{\text{max}}}$$
(6)

Understanding the behavior of the system is facilitated by a more compact approximation. When $[P]_o > 10K_{d2}$, which is reasonable under many conditions, one can find good approximations when either P or R is limiting.

When R is limiting ($[P]_o > [R]_o$), C_{max} is close to $[R]_o$ and one can write

$$EC_{50} \approx \frac{1}{2}[R]_{o} + \frac{[R]_{o}}{2[P]_{o} - [R]_{o}} K_{d2} + \frac{1}{\frac{[P]_{o} - \frac{1}{2}[R]_{o}}{K_{d2}} - 1} K_{d1}$$

When P is limiting $([R]_o > [P]_o)$, one can write a similar expression:

$$EC_{50} \approx \frac{1}{2} [P]_{o} + K_{d2} + \frac{1}{\frac{[R]_{o} - \frac{1}{2}[P]_{o}}{K_{d2}} - 1} K_{d1}$$
 (8)

These approximations afford insight into two fundamental features of the system. The first insight is that the sensitivity of the system is controlled more by K_{d2} than by ligand-receptor dissociation constant K_{d1} . While one can rigorously show that the normalized local objective sensitivity for K_{d2} is higher than that for K_{d1} under most conditions, it is more instructive to evaluate the effect on EC₅₀ for realistic values of other parameters. Figure 2B shows EC₅₀ as a function of K_{d1} , while Figure 2C shows EC₅₀ as a function of $K_{\rm d2}$. One observes for the K_{d1} dependence that there is a nearly linear correlation between EC_{50} and K_{d1} until K_{d1} reaches the low micromolar range. At this point, EC50 becomes rather insensitive to further changes in receptor-ligand affinity. By contrast, EC₅₀ strongly correlates with $K_{\rm d2}$ through its possible affinity range. Assuming nanomolar amounts of the receptor and protein, improvements in K_{d1} are necessary for the development of micromolar EC_{50} sensors but low values of K_{d2} are essential for developing nanomolar EC₅₀ sensors. Note that directed evolution of ligand-specific, highly sensitive sensors likely works by impacting both dissociation constants.

The second insight is the relative importance of the ratio between concentrations of receptor R and binding protein P, which we define as $r = [R]_o/[P]_o$. When P is limiting, this enables us to write the relationship

$$EC_{50} \approx \frac{1}{2} [P]_{o} + K_{d2} + K_{d1} \frac{1}{\frac{[P]_{o}}{K_{d2}} (r - \frac{1}{2}) - 1}$$
 (9)

Figure 2D plots EC₅₀ as a function of this ratio r when $[P]_o = 10K_{d2}$. There is an approximately 1/r dependence on EC₅₀ at low and moderate r values. At very high r values, the third term in eq 9 becomes small relative to the first two terms and EC₅₀ approaches the asymptote of $^1/_2[P]_o + K_{d2}$. When R is limiting, a similar finding of the 1/r dependence on EC₅₀ with the ratio r is now defined as $r = [P]_o/[R]_o$. However, note that the limiting asymptote for EC₅₀ for this configuration now becomes $^1/_2[R]_o$. Because K_{d2} is in the low nanomolar range for engineered molecular ratchets, this finding shows that configurations of ultrasensitive (picomolar-responsive) sensors for engineered

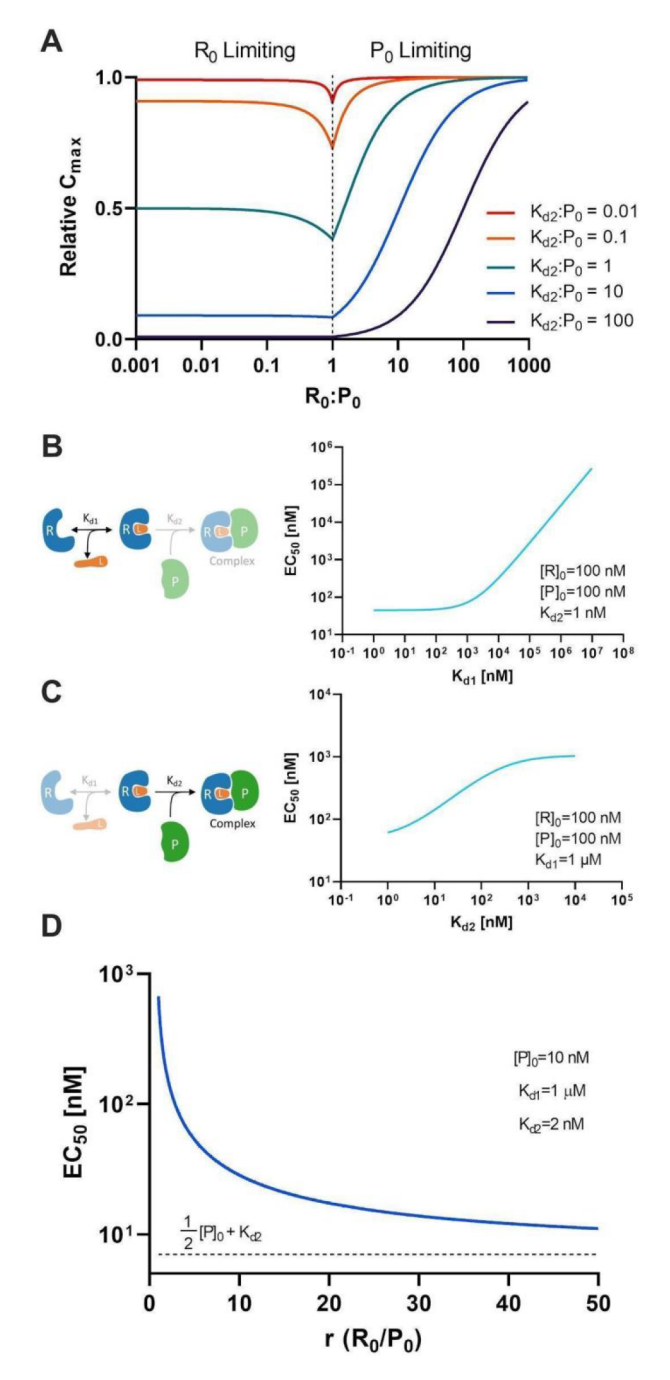


Figure 2. Molecular ratchet responsiveness and sensitivity. (A) Under saturating ligand conditions, the maximum complex normalized by limiting protein or receptor (relative C_{max}) is shown as a function of $[R]_{o}$, $[P]_{o}$, and K_{d2} . (B) The EC_{50} for molecular ratchets is strongly correlated with micromolar K_{d1} values but is relatively insensitive to changes at physiologically relevant nanomolar K_{d1} values. (C) Molecular ratchet EC_{50} s are correlated with K_{d2} over the physiologically relevant range. (D) High molar ratios of R_0 to P_0 correspond to a higher sensitivity of the system. Note that high ratios can correspond to an $EC_{50} > 100$ -fold lower than the corresponding dissociation constant for receptor recognition of the ligand (K_{d1}).

signaling pathways or *in vitro* applications should operate when R is limiting.

Receptor–Protein Complexation in the Absence of a Ligand. Naively, one would think to push EC_{50} as low as possible by tuning the molar ratio of one protein over the other to near infinite values. In practice, the receptor and protein can

Biochemistry pubs.acs.org/biochemistry Article

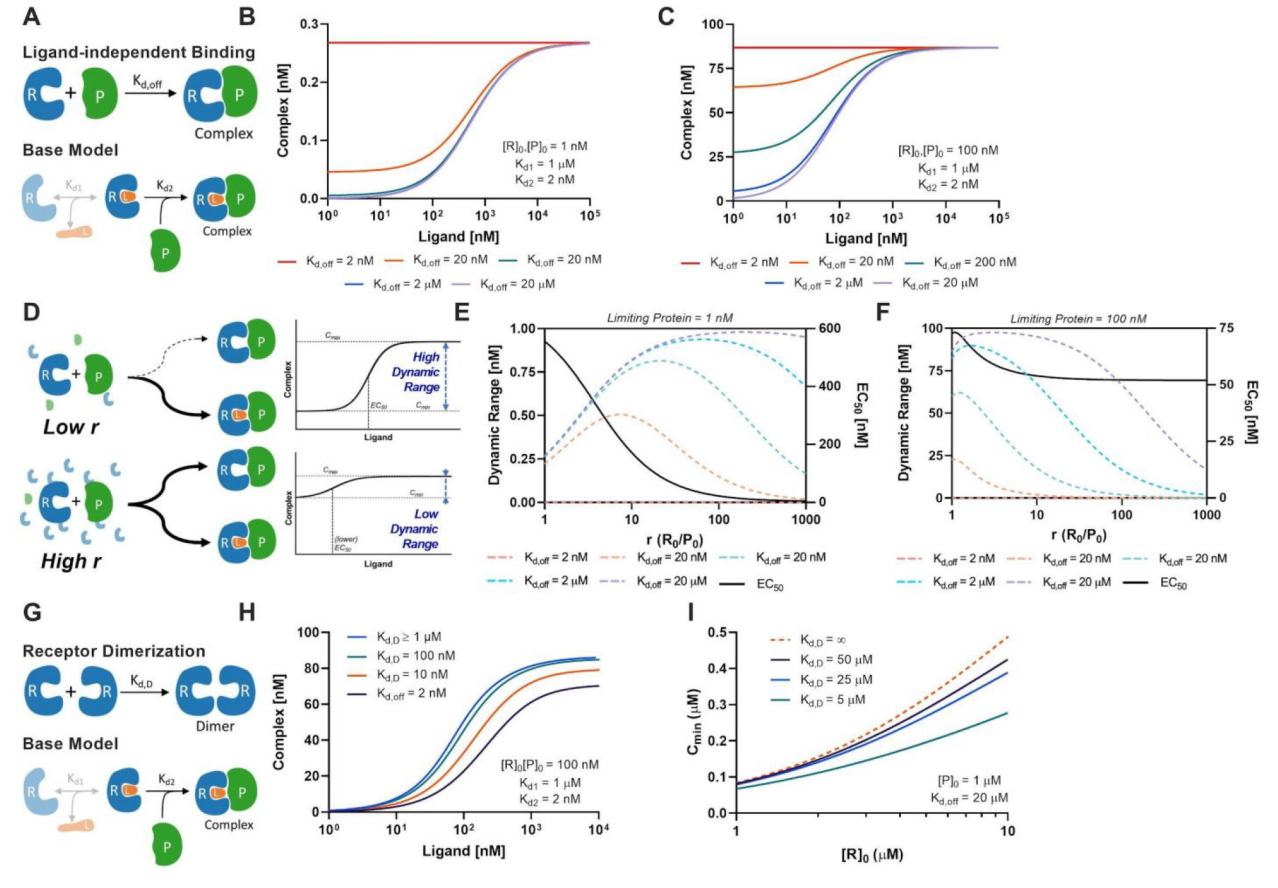


Figure 3. Molecular ratchet responses considering ligand-independent binding and receptor dimerization. (A) Schematic of ligand-independent complexation. (B and C) Transfer functions shown for $K_{\rm d,off}$ values ranging from 2 nM to 20 μ M at protein and receptor concentrations of 1 and 100 nM, respectively. (D–F) Dynamic ranges and EC $_{50}$ values are shown as a function of r. The dynamic range of the system is shown in color for a range of $K_{\rm d,off}$ values, while the EC $_{50}$ is colored black. Both outputs are plotted as a function of r, the ratio of excess to limiting protein, at (E) 1 nM and (F) 100 nM limiting protein. (G) Cartoon of the reaction network that includes receptor homodimerization. Receptor dimerization reduces the level of ligand-independent complexation without impacting sensitivity. (H) Transfer curves plotted as a function of $K_{\rm d,D}$. No changes in transfer curves exist as long as $K_{\rm d,D} > K_{\rm d,1}$. (I) $C_{\rm min}$ is shown as a function of [R] $_{\rm o}$ considering the base model, receptor dimerization, and ligand-independent binding. Physiologically relevant $K_{\rm d,D}$ values serve to reduce ligand-independent complexation ($C_{\rm min}$).

form a complex in the absence of the ligand, which impacts both the sensitivity and the dynamic range of the system. Let us define an additional term in the reaction network where this ligand-free receptor protein complex is controlled by dissociation constant $K_{\text{d,off}}$ (Figure 3A):

$$\mathbf{R} + \mathbf{P} \overset{K_{\mathrm{d,off}}}{\Longleftrightarrow} \mathbf{C}_{\mathrm{min}}$$

where C_{\min} represents the complex formed from this ligand-independent reaction. The C_{\max} for this reaction is unchanged relative to eq 3. However, C_{\min} is no longer zero:

$$C_{\min} = \frac{1}{2} \left[K_{\text{d,off}} + [R]_{\text{o}} + [P]_{\text{o}} - \sqrt{(K_{\text{d,off}} + [R]_{\text{o}} + [P]_{\text{o}})^{2} - 4[R]_{0}[P]_{0}} \right]$$
(10)

This equation shows that high concentrations of R and/or P drive complexation in the absence of the ligand, which leads to constitutive interactions and a lowered dynamic range of outputs. This implication is particularly important for *in vivo* applications, as described in Sensitivity and Responsiveness for In Vivo Molecular Ratchets.

We can also solve, as before, for the ligand concentration for a given [C]:

$$[L]_{o} = [C] + \frac{[C]}{[P]_{o} - [C]} K_{d2}$$

$$+ K_{d1} \frac{\frac{[C]}{[P]_{o} - [C]} K_{d2}}{[R]_{o} - \frac{[C]}{[P]_{o} - [C]} K_{d2} - [C]} \left(1 - \frac{K_{d2}}{K_{d,off}}\right)$$

$$- \left(\frac{K_{d1} K_{d2}}{K_{d,off}}\right) + \left(\frac{K_{d2} + [P]_{o}}{K_{d,off} - K_{d2}}\right)$$

$$\left([R]_{o} - \frac{[C]}{[P]_{o} - [C]} K_{d2} - [C]\right)$$
(11)

The equation described above collapses to eq 4 in the limit of $K_{\rm d,off} \rightarrow \infty$. Panels B and C of Figure 3 show how varying $K_{\rm d,off}$ values affect the transfer functions for complex formation. Figure 3B shows the transfer function for low R and P concentrations; minimal changes result except in the limit as $K_{\rm d,off}$ approaches $K_{\rm d2}$. Figure 3C shows the transfer function for concentrations of R and P roughly consistent with *in vivo* applications. Here one clearly sees the impact of ligand-independent binding. While EC₅₀ and $C_{\rm max}$ are independent for all $K_{\rm d,off} > K_{\rm d2}$, the dynamic range ($C_{\rm max}$ to $C_{\rm min}$) becomes severely limited even under low micromolar $K_{\rm d,off}$ values. Thus, dynamic ranges necessary for

reasonable *in vivo* applications require $K_{\rm d,off}$ values of micromolar or higher.

With ligand-independent binding, changes in ratio r come with a trade-off: an increasing r increases C_{\max} at the expense of increasing C_{\min} (Figure 3D). We can calculate the optimal ratio necessary to maximize the dynamic range by taking a partial derivative of the dynamic range with respect to r and solving for zero. The resulting expression is given:

$$r(\text{maximum dynamic range}) = 1 + \sqrt{\frac{K_{\text{d,off}}K_{\text{d2}}}{[P]_{\text{o}}2}}$$
 (12)

For realistic values ($K_{\rm d,off}=10~\mu{\rm M}$; $K_{\rm d2}=2~{\rm nM}$; [P]_o = 100 nM), this equation suggests an optimal r of approximately 2.5 to maximize the dynamic range. However, r also improves the sensitivity by decreasing EC₅₀. What is the optimal r that maximizes the dynamic range and minimizes EC₅₀? Panels E and F of Figure 3 show the impact of r on the dynamic range and EC₅₀ for low [[P]_o = 1 nM (Figure 3E)] and high [[P]_o = 100 nM (Figure 3F)] concentrations of the limiting protein. For low [P]_o values and reasonable $K_{\rm d,off}$ values, higher values of r decrease EC₅₀ without appreciably impacting the dynamic range until the excess protein is close to the micromolar concentration. Thus, for many *in vitro* applications, one can operate under r ratios of 100 or more to maximize sensitivity. For higher [P]_o values likely *in vivo*, the dynamic range plateau is much narrower, and the multiobjective optimal r is closer to 5–10 (Figure 3F).

Effect of Receptor Dimerization. Some natural receptor proteins are known to dimerize, with or without bound hormones.¹⁸ For the sake of simplicity, we will assume all three possible dimerization reactions have the same dissociation constant $K_{d,D}$, although it is known that ABA receptors have subtle but significant K_d differences depending on hormone occupancy. 18 Here we consider the molecular ratchet system with this dimerization but without ligand-independent binding (Figure 3G). While we can solve for the closed form solution of the transfer function, the actual expression is too unwieldy for useful analysis. Instead, Figure 3H shows the effect of such dimerization on transfer functions. As shown in the graph, there is little impact on the shape of the transfer function whenever $K_{\rm d,D}/K_{\rm d1} > 1$ and substantial impacts on responsiveness only when $K_{\rm d.D}/K_{\rm d1}\ll 1$. Because PYL2 and related dimeric ABA receptors have reported natural $K_{\rm d,D}$ values roughly similar to $K_{\rm d,1}$ values, ^{18,19} dimerization has little impact on EC₅₀. However, dimerization can function by drawing away a pool of potential monomeric receptors that can form the ligand-independent complex. Figure 3I shows the impact of C_{\min} considering both ligand-independent and dimerization side reactions. This dimerization activity can reduce background (C_{min}) for high nanomolar to low micromolar concentrations of proteins. Reducing C_{\min} is especially important for the removal of the constitutive activity of genetic circuits as we will discuss in Sensitivity and Responsiveness for In Vivo Molecular Ratchets.

Interpretation of Molecular Ratchet *In Vitro* Binding Isotherms. The sensitivity of molecular ratchets *in vitro* has been quantified using isothermal calorimetry (ITC), ^{13,19,20} yeast surface display titrations, ¹⁴ ELISA-like microplate assays, ¹¹ surface plasmon resonance measurements, ^{13,21} and competitive inhibition IC₅₀ measurements. ²² In this section, we first derive limiting equations suitable for determining equilibrium dissociation constants using yeast surface display titrations and surface plasmon resonance (SPR)/biolayer interferometry (BLI). Next, we derive useful EC₅₀ values for ELISA-like

microplate assays that are relevant for drug and toxicology screening assays. Finally, we derive the IC_{50} found by the phosphatase assays in terms of the underlying kinetic rate parameters and concentrations of proteins used in the assay.

In Vitro Determination of Equilibrium Dissociation Constants K_{d1} and K_{d2} . Equilibrium dissociation constants K_{d1} and K_{d2} have been measured by yeast cell surface titration and by surface plasmon resonance. Note that K_{d1} can also be fit directly using ITC measurements¹³ of the binary interaction between the monomeric hormone receptor and ligand; derivation of the K_{d3} by ITC measurement of ternary complex formation is much more complicated and beyond the scope of this work.

In yeast surface display titrations, 14 the hormone receptor is displayed on the surface of yeast and labeled simultaneously with ligand and biotinylated binding protein. After secondary labeling with a streptavidin-conjugated fluorophore, the samples are read by flow cytometry. The fluorescence associated with the secondary fluorophore is quantified as a function of the concentrations of the ligand and binding protein. Analysis of this set of measurements is used to infer the $K_{\rm d1}$ and $K_{\rm d2}$ dissociation rate constants. One important outcome from both yeast display and SPR measurements is that dissociation constant $K_{\rm d2}$ can be directly measured under the appropriate labeling conditions.

Consider the limiting case in which saturating amounts of ligand are added to the labeling reaction mixture. When $[P]_o/[R]_o > 10$, one finds that the amount of receptor labeled collapses to the previously described eq 3. This experiment will result, when $[P]_o$ is the independent variable, in a saturable isotherm that can be solved directly for $K_{\rm d2}$. The major consideration in developing this assay is to perform labeling conditions under which the hormone receptor is saturated with the ligand. As an example of the needed ligand amounts, let us consider the ligand concentration necessary for 95% of $C_{\rm max}$ when $[P]_o$ is equal to $K_{\rm d2}$. We can write the nearly exact expression required:

$$[L]_{o} \approx K_{d1} \left(\frac{0.95C_{\text{max}} \frac{K_{d2}}{[P]_{o}}}{[R]_{o} - 0.95C_{\text{max}} \frac{K_{d2}}{[P]_{o}} - 0.95C_{\text{max}}} \right) = 19K_{d1}$$
(13)

Because typical reported $K_{\rm d1}$ values are in the range of 0.5–5 $\mu\rm M$, 13,23 labeling concentrations then are typically on the order of 10–100 $\mu\rm M$ to ensure near saturation of the hormone receptor with the ligand.

Under appropriate experimental conditions, dissociation constant K_{d1} can be indirectly measured. When $[L]_o \gg [R]_o$ and $[P]_o \gg [R]_o$, we can derive the following expression:

$$C = C_{\text{max}} \left(\frac{[L]_{\text{o}}}{K_{\text{d,eff}} + [L]_{\text{o}}} \right)$$
(14)

where

$$K_{d,eff} = \frac{K_{d1}K_{d2}}{K_{d2} + [P]_{o}}$$
(15)

Performing titrations, when $[L]_o$ is the independent variable, allows us to determine K_{d1} indirectly by fitting first the isotherm for $K_{d,eff}$ and then inferring K_{d1} , where K_{d2} and $[P]_o$ are known. More accurate measurements result when multiple isotherms are performed at different $[P]_o$ values and K_{d1} fit using global nonlinear curve fitting.

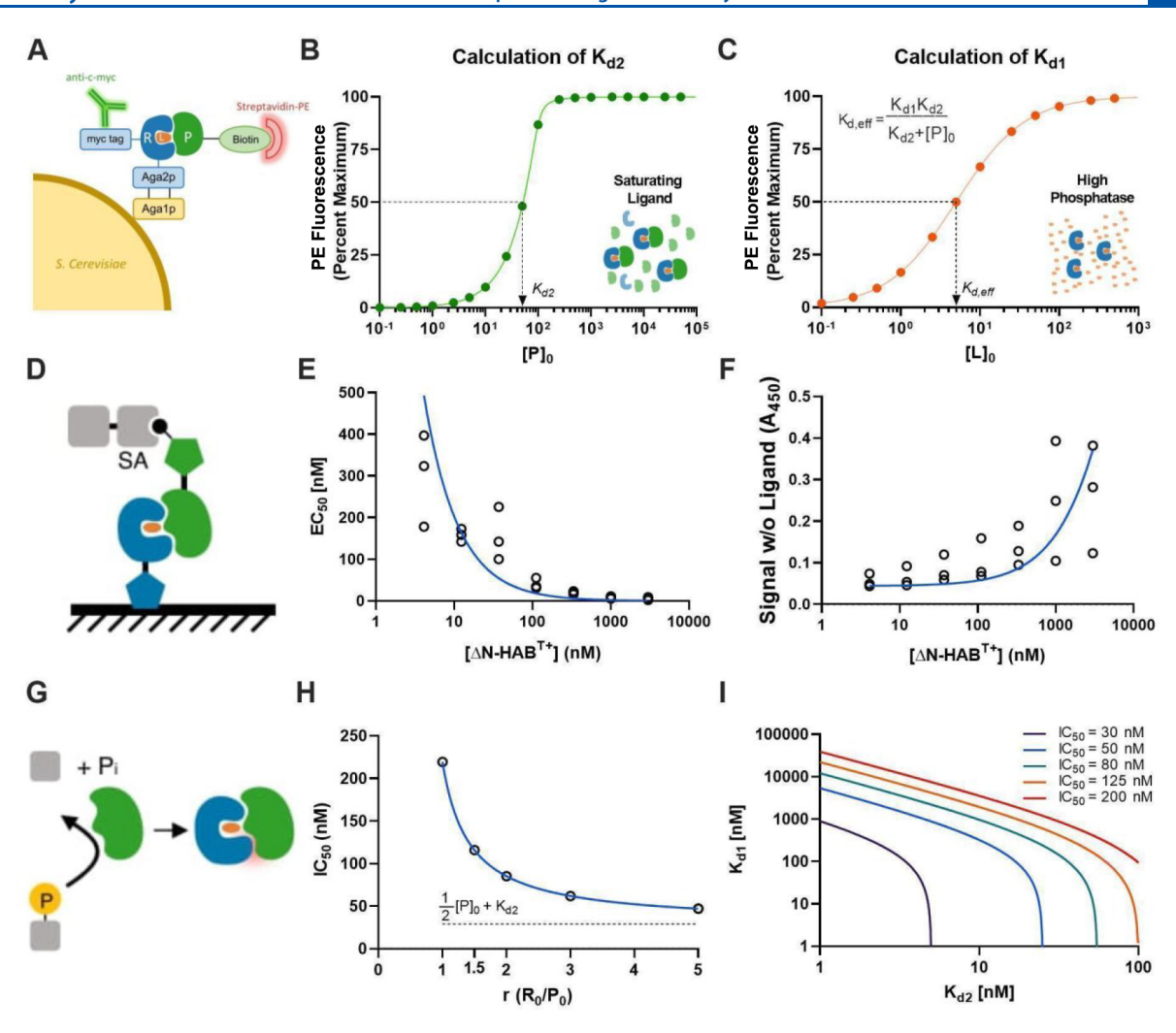


Figure 4. *In vitro* measurements of molecular ratchet parameters. (A) Cartoon of the yeast surface display (YSD) system showing the ternary complex translocated to the surface of *Saccharomyces cerevisiae*, bound with a fluorescent antibody and streptavidin. (B). Determination of $K_{\rm d2}$ via titration of the protein concentration in the presence of saturating ligand concentrations. (C) Determination of $K_{\rm deff}$ via titration of the ligand in the presence of saturating protein concentrations. $K_{\rm d1}$ can be inferred from the embedded equation. (D) Cartoon of the PYR1 ELISA-like immunoassay. Here, the receptor is immobilized and binds biotinylated HAB1 in the presence of the ligand. (E) EC₅₀ values for an ABA sensor are plotted as a function of [P]₀ (here ΔN-HAB1^{T+}) using data from ref 11. The curve fit to the data is of the form EC₅₀ = $K_{\rm d1}K_{\rm d2}/[P]_{\rm 0}$. (F) Background absorbance measurements were collected and plotted as a function of [P]₀, from the same data set utilized in panel E. The curve fit to the data is of the form $A_{\rm 450} = S \frac{[P]_{\rm 0}}{K_{\rm d,off} + [P]_{\rm 0}}$, where S is an arbitrary scalar conversion. (G) Cartoon of ligand-dependent phosphatase inhibition unique to the PYR1/HAB1 system. (H) IC₅₀ decreases as a function of receptor/protein ratio r. (I) IC₅₀ isoclines are plotted for different $K_{\rm d1}$ and $K_{\rm d2}$ values.

One limiting consideration for *in vitro* measurements using surface display is that the local concentration of receptors is so high that even weakly dimeric receptors associate on the cell surface and thus prevent recruitment of ligand and binding protein. ¹⁴ Thus, only monomeric receptors can be assessed using display techniques.

Experimentalists using SPR/BLI can use the governing equations presented above to determine $K_{\rm d1}$ and $K_{\rm d2}$ under experimental conditions where R is immobilized. To determine $K_{\rm d2}$, note that saturating amounts of the ligand must be added to all wash and equilibration buffers. To determine $K_{\rm d,eff}$, equilibrium analysis is recommended as the kinetics of ternary complex formation may be too complex for accurate fitting of monovalent binding kinetic rate constants.

ELISA-like Microplate Assays. In the ELISA-like microplate assays developed by Beltran et al., 11 receptor R is immobilized on microtiter plates, with biotinylated protein P and ligand L added to wells simultaneously (Figure 4D). Detection of the

ternary complex occurs using a streptavidin-linked horseradish peroxidase. The amount of R immobilized in a conformation allowing complex formation is unknown but is likely to be in the picomolar range. We found for this system that P could be added in great excess of R, resulting in low EC_{50} values and picomolar limits of detection in complex biological matrices. Under these conditions, we can simplify eq 7 to approximate the EC_{50} :

$$EC_{50} \approx \frac{1}{2} [R]_{o} + \frac{K_{d1} K_{d2}}{[P]_{o}}$$
 (16)

However, micromolar amounts of P drive complexation and high background in the absence of ligand according to eq 10. When $[R]_o \ll [P]_o$, which is the case in this system, eq 10 reduces to

$$\frac{C_{\min}}{\left[\mathrm{R}\right]_{\mathrm{o}}} = \frac{\left[\mathrm{P}\right]_{\mathrm{o}}}{K_{\mathrm{d,off}} + \left[\mathrm{P}\right]_{\mathrm{o}}} \tag{17}$$

Thus, there is some trade-off between sensitivity and ligandindependent binding minimizing the dynamic range. Panels E and F of Figure 4 show the optimization data, originally reported in ref 11, for a monomerically engineered PYR1 sensing ABA. Figure 4E shows experimentally determined EC₅₀ values as a function of a thermally stabilized binding protein (ΔN -HAB1^{T+}) and a fitted line using eq 16. The one-parameter fit gives a $K_{d1}K_{d2}$ value of 2020 nM², which is order of magnitude consistent with previous measurements (e.g., $K_{d2} = 2$ nM, and $K_{\rm d1}$ = 1010 nM). Figure 4F shows the experimental background absorbance values at 450 nm (A_{450}) in the absence of the ligand. Equation 17 is fit using one parameter $(K_{d,off})$ along with an arbitrary scaling factor to convert to A_{450} . Reasonable agreement between experiments and our calculations results with a $K_{\text{d.off}}$ of 14.5 μ M. Thus, for this system, we found a [P]_o of 1–5 μ M to give the right balance between manageable ligand-independent binding and maximum sensitivity. However, the optimal P concentration for different molecular ratchets will strongly depend on its particular $K_{\text{d.off}}$, which must be empirically determined.

Interpretation of IC_{50} Measurements with Respect to K_{d1} and K_{d2} . In some natural systems, binding protein P is an enzyme, and complex formation results in competitive inhibition. In the specific case of the ABA receptors PYR, PYL, and RCAR, sensitivities of natural and engineered receptors to different controlling ligands are often assessed using phosphatase inhibition of PP2C HAB1, with a 50% inhibitory concentration (IC₅₀) as the measurement (Figure 4G). Because 50% of complex formation results in 50% loss of enzyme activity, here IC50 is equivalent to EC50. The major challenge of such inhibition assays is interpreting IC50 measurements relative to the underlying dissociation constants for the elementary rate steps. Because increasing the amount of R relative to PP2C decreases the observed IC50 values under typical assay conditions (Figure 4H), small differences in the activity of recombinant proteins from purifications can result in substantial differences in the IC50 measurement. Thus, it is important to measure the percent active receptor using an independent assay.²² Our closed form model can also be used to identify the set of K_{d1} and K_{d2} values that are consistent with different IC₅₀s. Figure 4I shows isoclines for IC₅₀ values ranging from 30 to 200 nM under common conditions for the inhibition assay ([PP2C] = 50 nM; [PYR1] = 250 nM). We observe a wide range of $K_{\rm d1}$ values consistent with each IC₅₀. For example, the $K_{\rm d1}$ could range from 50 nM to >5 μ M for the same IC₅₀ value of 50 nM. Note also that $K_{\rm d2}$ becomes increasingly important as IC₅₀ values inch closer to the theoretical minimum of 25 nM $(^{1}/_{2}[PP2C])$, where K_{d2} must be at most 4 nM for an IC₅₀ of 30 nM.

Sensitivity and Responsiveness for *In Vivo* Molecular Ratchets. *In vivo* engineering and basic biology applications for molecular glues and molecular ratchets have been covered by several excellent reviews. ^{1,2} A majority of applications have two different genetic architectures. The first architecture involves transcriptional activation of a gene of interest by separating a DNA binding domain (DBD) from a transcriptional activation domain (TA). Addition of a ligand recruits the TA domain to the DBD, driving expression of the gene of interest. The second architecture is fusion of the receptor and binding proteins to different portions of a split protein. Ligand-dependent complexation reconstitutes the split protein. Finally, a special use case involves both architectures. T7 RNA polymerase (T7 RNAP) is a single-subunit RNA polymerase and has previously been

engineered as a split protein.²⁴ Reconstitution of the full-length T7 RNAP drives transcriptional activation.

In this section, we consider the general features of the equilibrium sensitivity and responsiveness for the different configurations described above. There are several limitations in our equilibrium analysis. One major issue is that time scales for equilibrium in living cells can be on the order of tens of hours owing to time sinks related to the low permeability of the controlling ligand across cell membranes, active transport of the ligand outside of cells, gene synthesis rates, protein degradation and dilution by cell growth, maturation of the protein to its active form, and compartmental protein trafficking. Forward engineering requires integration of molecular ratchet binding equilibria with a full gene expression model, including these and other cell- and system-specific terms. Nevertheless, the base models are general enough that they should provide useful insight to the synthetic biologist.

Transcriptional Activation by Fusion to DNA Binding and Transcriptional Activation Domains. A common transcriptional activation configuration is fusing one-half of a molecular ratchet to where one protein is fused to a DBD and the other to a TA (Figure 5A). This configuration is the basis for yeast two-hybrid selections used for identifying new sensors ¹⁰ and has also

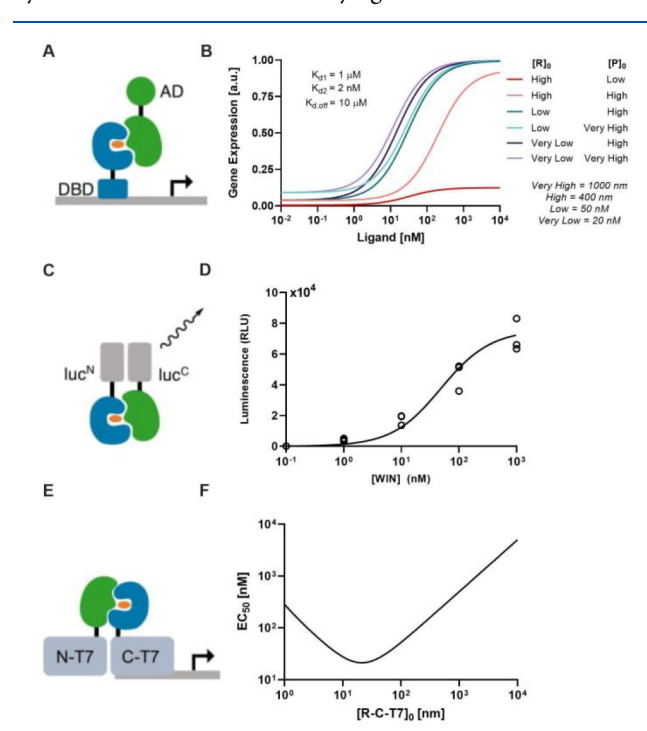


Figure 5. Tuning *in vivo* applications for sensitivity and dynamic range. (A) Cartoon of the ligand-induced transcriptional activation using the split DBD and AD. (B) Gene expression (arbitrary units) is shown as a function of various sets of initial conditions. The maximum sensitivity is observed when the level of expression of the receptor—DBD fusion is very low and that of the protein—AD fusion is very high, albeit at the expense of a higher background. (C) Cartoon of the ligand-induced reconstitution of split proteins. Here a split luciferase system is shown. (D) Ligand-dependent reconstitution of NanoLuc luciferase using data from ref 11. The curve fit to the data uses eq 7 with the following values: [R] $_{\rm o} = 50$ nM, [P] $_{\rm o} = 20$ nM, $K_{\rm d1} = 836$ nM, and $K_{\rm d2} = 2$ nM. (E) Cartoon of split T7 RNAP. (F) EC $_{\rm 50}$ plotted as a function of receptor—C-T7 fusion protein. Here, [P] $_{\rm o}$ /[R] $_{\rm o} = 10$, $K_{\rm d1} = 1$ μ M, and $K_{\rm d2} = 2$ nM. Note that EC $_{\rm 50}$ becomes linearly proportional to the receptor—C-T7 fusion above 100 nM.

been used in mammalian applications.^{6,7} The dynamics and output of gene expression depend on the molecular ratchet parameters as well as the binding dissociation constant between the DBD and its cognate DNA recognition sequence (K_G) , and the number of DBD binding sites in the promoter ([G]). For the sake of simplicity, we assume that binding dissociation constant K_G is identical for the DBD alone and when complexed with the AD. We also assume that [G] (number of DNA recognition sequences per cell) is much smaller than the number of DBD fusion proteins. As shown below, this is a very good assumption for almost all eukaryotic systems. Another assumption is that we disregard the effect of nuclear localization sequences (NLS) on the recruitment of the holocomplex to the nucleus. Finally, we define activity as proportional to the fraction of [G] occupied with an AD times the number of copies of G per cell. This definition leads to the following expression:

gene expression
$$\propto$$
 [G] $\frac{[C]}{K_G + [DBD \text{ fusion}]_o}$ (18)

Analysis requires estimation of per cell protein abundance. Margeurat et al. ²⁵ measured the quantitative abundance of the fission yeast proteome, yielding a median of 200 and a range of $256-1.05\times10^6$ proteins per cell. Given that a typical diameter of fission yeast is 6 μ m, 2000 proteins will correspond to an approximate intracellular concentration of 30 nM. At the high end of the range is ADH1 with approximately 5×10^5 proteins per cell. As many common Y2H configurations use ADH1 promoters, we can reasonably infer that the concentration of molecular ratchet partners is >30 nM, although exact abundances are difficult to quantify. Even still, the dissociation constant K_G for typical DBD sequences used is much \ll 30 nM, 26 leading to the following simplified expression:

gene expression
$$\propto \frac{[C]}{[DBD \text{ fusion}]_0}$$
 (19)

Figure 5B plots potential transfer functions under different expression levels for the same molecular ratchet subsystem where the receptor is fused to the DBD and binding protein P is fused to the AD. Because one is unable to precisely tune the protein concentration, one modulates protein expression by tuning the promoter expression strength qualitatively (e.g., promoters of strength very low, low, medium, and high). Application of eq 19 has several intuitive implications for maximizing responsiveness (C_{max}), minimizing EC₅₀, and minimizing the signal in the absence of the ligand (C_{\min}) . First, the protein fused to the DBD must be limiting for maximum responsiveness; in the high-R, low-P case, there is little signal responsiveness, whereas all cases where R is limiting show low nanomolar EC₅₀ values and near maximal responsiveness. Second, EC50 is minimized and responsiveness is maximized when the level of expression of the R-DBD fusion protein is as low as possible while the level of expression of the P-AD fusion protein is as high as possible. Our model predicts \geq 20-fold shifts in EC₅₀ when this ratio is changed. Finally, this maximum responsiveness and low EC50 come with a trade-off of higher basal activity in the absence of the ligand (Figure 5B). Thus, applications in which the background must be minimized require tuning of the expression to suboptimal EC₅₀ values.

For Y2H and other growth-based assays, phenotypic coupling to gene expression is nonlinear as fractional occupation by the DBD-AD complex of $\ll 1$ could result in a maximum specific growth rate. The exact details will be system-specific, but the end

ı

result will almost always be that the observed EC_{50} in such growth-based assays will be lower than the EC_{50} predicted from the full model shown in Figure 5B. This is particularly important when the individual proteins are expressed at high nanomolar or low micromolar concentrations, as is likely under typical Y2H setups. Thus, our model sets a ceiling on the EC_{50} observed for certain genetic configurations.

Signal Transduction from Reconstitution of a Split Protein. Chemical biologists and biotechnologists extensively use split proteins, in which a useful function (catalysis, binding, fluorescence, or luminescence) is encoded by individually inactive pieces. In this context, molecular ratchets and glues work by forming a ternary complex that places inactive pieces in the proximity, increasing their local concentration. This high local concentration reconstitutes the split pieces into the full-length protein, restoring activity (Figure 5C).

There are two issues confounding the direct translation of the molecular ratchet model to predict signal transduction for split proteins. First, the activity in the absence of the ligand depends on transient association of the split pieces as well as ligand-independent complexation. This transient association can be modeled using a dissociation constant between the two pieces, but this value has been measured only rarely for cases such as NanoBiT.²⁷ Second, the restored activity when the ternary complex has formed depends on the increase in the local or effective concentration of the two split pieces. This local concentration depends on system-specific parameters like linker lengths, relative orientations of the split proteins and molecular ratchet pieces, sizes of the components, and distances between the biomolecules.

What results then is that the $C_{\rm min}$ and $C_{\rm max}$ of the response are a function of not only the dynamics of the molecular ratchet but also the system-specific details noted above; thus, the CID model cannot predict these parameter values. However, the EC₅₀ is unchanged from eqs 6–8, and thus, our closed form model can predict the sensitivities of the transfer functions for split proteins *in vivo*. For example, Beltran et al. used a split NanoLuc system fused to a PYR1-based sensor to sense the synthetic cannabinoid WIN 55,212-27 with an EC₅₀ of 56 nM. Our closed form model can recapitulate the luciferase—ligand transfer curve using reasonable parameters based on the sensitivity of the sensor and the likely expression levels of the two split fusion partners (Figure 5D).

Reconstitution of Split T7 RNA Polymerase. A final special case involving transcriptional activation of a split protein involves split T7 RNAP (Figure 5E). In this system, a C-terminal half (C-T7) encodes catalytic function and promoter recognition. The N-terminal half (N-T7) encodes a portion of the polymerase essential for converting T7 RNAP from the initiation to an elongation complex; in the absence of N-T7, C-T7 can bind at T7 DNA promoters and initiate transcription but produces only abortive transcripts. The Dickinson lab has developed this split T7 system coupled to molecular ratchets for use as general purpose biosensors, and other laboratories have used similar architectures for sense and response applications. These bacterial sensors have observed responsiveness in the micromolar range, even though the same sensors in other configurations can have picomolar limits of detection. To understand why, we can derive an expression similar to eq 18:

gene expression
$$\propto [G] \frac{[C]}{K_G + [C-T7 \text{ fusion}]_0}$$
 (20)

Biochemistry pubs.acs.org/biochemistry Article

Equation 20 is derived using two fundamental assumptions. The first is that the gene copy number [G] is much lower than the C-T7 fusion protein concentration. This assumption may fail in prokaryotic expression systems where one molecule is approximately 1 nM intracellularly, 31 as medium-copy plasmids encode mid-nanomolar values for [G]. Second, we assume that activation of gene expression does not impact growth rates, but overexpression of unregulated T7 RNAP is well-known to cause the cessation of growth. Thus, eq 20 should strictly be used when the number of gene copies per cell is 1-2. Even considering that eq 20 is limited by these two assumptions, examination leads to a rationale for the observed micromolar sensitivities of these sensors. Figure 5F shows EC₅₀ as a function of C-T7 protein concentration. For reasonable sensor dissociation constants, EC₅₀ becomes linearly proportional to C-T7 abundance. Therefore, a likely explanation for micromolar responsiveness for these bacterial sensors is that the expression level of these proteins at thousands of copies per cell sets the perceived affinity limit.

Our analysis also provides several useful insights for the molecular engineer. First, because C-T7 is in the denominator for eq 20, the protein fused to C-T7 should be expressed at levels lower than that of the N-T7 protein fusion. Second, the model predicts that the level of expression of the C-T7 fusion protein should be as low as possible to minimize the EC $_{50}$. For prokaryotes, this translates to <100 copies per cell and requires optimization using weak promoters, ribosome binding site strengths, and protein degradation tags. Finally, the model predicts that the N-T7 fusion protein should be in approximately 10-fold excess versus the C-T7 fusion protein to minimize ligand-independent complexation.

CONCLUSION

Here we have developed a closed form model for a distinct CID module we term molecular ratchets. Molecular ratchets engage in saturable binding kinetics and are characterized well by a Hill equation with minimal cooperativity observed under most conditions. Useful governing equations for a variety of *in vitro* and *in vivo* applications are derived, and experimental fits to published data sets show excellent agreement between the model and experiment.

AUTHOR INFORMATION

Corresponding Author

Timothy A. Whitehead — Department of Chemical and Biological Engineering, University of Colorado Boulder, Boulder, Colorado 80305, United States; ⊙ orcid.org/0000-0003-3177-1361; Phone: +1 (303)-735-2145; Email: timothy.whitehead@colorado.edu

Authors

Paul J. Steiner – Department of Chemical and Biological Engineering, University of Colorado Boulder, Boulder, Colorado 80305, United States

Samuel D. Swift — Department of Chemical and Biological Engineering, University of Colorado Boulder, Boulder, Colorado 80305, United States

Matthew Bedewitz — Department of Chemical and Biological Engineering, University of Colorado Boulder, Boulder, Colorado 80305, United States

Ian Wheeldon — Institute for Integrative Genome Biology and Department of Chemical and Environmental Engineering, University of California Riverside, Riverside, California 92521, United States

Sean R. Cutler – Institute for Integrative Genome Biology, Department of Botany and Plant Sciences, and Center for Plant Cell Biology, University of California Riverside, Riverside, California 92521, United States

Dmitri A. Nusinow – Donald Danforth Plant Science Center, St. Louis, Missouri 63132, United States

Complete contact information is available at: https://pubs.acs.org/10.1021/acs.biochem.2c00172

Funding

This work was supported by Defense Advanced Research Projects Agency Advanced Plant Technologies (DARPAAPT, HR001118C0137, to D.A.N., T.A.W., S.R.C., and I.W.) and National Science Foundation Grants 2128287 to T.A.W. and 2128016 to S.R.C. and I.W.

Notes

The authors declare no competing financial interest. All scripts and raw data used to generate the figures are available as R, MATLAB, or Graphpad Prism files and are available from the WhiteheadGroup Github under folder "ACS-Biochemistry-Steiner-2022".

REFERENCES

- (1) Stanton, B. Z.; Chory, E. J.; Crabtree, G. R. Chemically induced proximity in biology and medicine. *Science* **2018**, *359*, eaao5902.
- (2) Schreiber, S. L. The Rise of Molecular Glues. Cell 2021, 184, 3–9.
- (3) Cao, S.; Kang, S.; Mao, H.; Yao, J.; Gu, L.; Zheng, N. Defining molecular glues with a dual-nanobody cannabidiol sensor. *Nat. Commun.* **2022**, *13*, 815.
- (4) Douglass, E. F., Jr; Miller, C. J.; Sparer, G.; Shapiro, H.; Spiegel, D. A. A comprehensive mathematical model for three-body binding equilibria. *J. Am. Chem. Soc.* **2013**, *135*, 6092–6099.
- (5) Hejátko, J., Hakoshima, T., Eds. Plant Structural Biology: Hormonal Regulations; Springer: Cham, Switzerland, 2018.
- (6) Liang, F.-S.; Ho, W. Q.; Crabtree, G. R. Engineering the ABA plant stress pathway for regulation of induced proximity. *Sci. Signaling* **2011**, *4*, rs2.
- (7) Ziegler, M. J.; Yserentant, K.; Middel, V.; Dunsing, V.; Gralak, A. J.; Pakari, K.; Bargstedt, J.; Kern, C.; Chiantia, S.; Strähle, U.; Herten, D.-P.; Wombacher, R. A chemical strategy to control protein networks in vivo. *bioRxiv* **2020**, DOI: 10.1101/2020.04.08.031427.
- (8) Miyamoto, T.; DeRose, R.; Suarez, A.; Ueno, T.; Chen, M.; Sun, T.-P.; Wolfgang, M. J.; Mukherjee, C.; Meyers, D. J.; Inoue, T. Rapid and orthogonal logic gating with a gibberellin-induced dimerization system. *Nat. Chem. Biol.* **2012**, *8*, 465–470.
- (9) Wu, C.-Y.; Roybal, K. T.; Puchner, E. M.; Onuffer, J.; Lim, W. A. Remote control of therapeutic T cells through a small molecule—gated chimeric receptor. *Science* **2015**, *350*, aab4077.
- (10) Park, S.-Y.; Peterson, F. C.; Mosquna, A.; Yao, J.; Volkman, B. F.; Cutler, S. R. Agrochemical control of plant water use using engineered abscisic acid receptors. *Nature* **2015**, *520*, 545–548.
- (11) Beltrán, J.; Šteiner, P. J.; Bedewitz, M.; Wei, S.; Peterson, F. C.; Li, Z.; Hughes, B. E.; Hartley, Z.; Robertson, N. R.; Medina-Cucurella, A. V.; Baumer, Z. T.; Leonard, A. C.; Park, S.-Y.; Volkman, B. F.; Nusinow, D. A.; Zhong, W.; Wheeldon, I.; Cutler, S. R.; Whitehead, T. A. Plant hormone receptors as reprogrammable scaffolds for rapid biosensor development. *Nat. Biotechnol.* **2022**, DOI: 10.1038/s41587-022-01364-5.
- (12) Melcher, K.; Ng, L.-M.; Zhou, X. E.; Soon, F.-F.; Xu, Y.; Suino-Powell, K. M.; Park, S.-Y.; Weiner, J. J.; Fujii, H.; Chinnusamy, V.; Kovach, A.; Li, J.; Wang, Y.; Li, J.; Peterson, F. C.; Jensen, D. R.; Yong, E.-L.; Volkman, B. F.; Cutler, S. R.; Zhu, J.-K.; Xu, H. E. A gate-latch-lock mechanism for hormone signalling by abscisic acid receptors. *Nature* **2009**, *462*, 602–608.

- (13) Dupeux, F.; Santiago, J.; Betz, K.; Twycross, J.; Park, S.-Y.; Rodriguez, L.; Gonzalez-Guzman, M.; Jensen, M. R.; Krasnogor, N.; Blackledge, M.; Holdsworth, M.; Cutler, S. R.; Rodriguez, P. L.; Márquez, J. A. A thermodynamic switch modulates abscisic acid receptor sensitivity. *EMBO J.* **2011**, *30*, 4171–4184.
- (14) Steiner, P. J.; Bedewitz, M. A.; Medina-Cucurella, A. V.; Cutler, S. R.; Whitehead, T. A. A yeast surface display platform for plant hormone receptors: Toward directed evolution of new biosensors. *AIChE J.* **2020**, *66*, e16767.
- (15) Dupeux, F.; Antoni, R.; Betz, K.; Santiago, J.; Gonzalez-Guzman, M.; Rodriguez, L.; Rubio, S.; Park, S.-Y.; Cutler, S. R.; Rodriguez, P. L.; Márquez, J. A. Modulation of abscisic acid signaling in vivo by an engineered receptor-insensitive protein phosphatase type 2C allele. *Plant Physiol.* **2011**, *156*, 106–116.
- (16) Murase, K.; Hirano, Y.; Sun, T.-P.; Hakoshima, T. Gibberellin-induced DELLA recognition by the gibberellin receptor GID1. *Nature* **2008**, 456, 459–463.
- (17) Dane Wittrup, K.; Tidor, B.; Hackel, B. J.; Sarkar, C. A. Quantitative Fundamentals of Molecular and Cellular Bioengineering; MIT Press: Cambridge, MA, 2020.
- (18) Zhang, X.; Zhang, Q.; Xin, Q.; Yu, L.; Wang, Z.; Wu, W.; Jiang, L.; Wang, G.; Tian, W.; Deng, Z.; Wang, Y.; Liu, Z.; Long, J.; Gong, Z.; Chen, Z. Complex structures of the abscisic acid receptor PYL3/RCAR13 reveal a unique regulatory mechanism. *Structure* **2012**, *20*, 780–790.
- (19) Hao, Q.; Yin, P.; Li, W.; Wang, L.; Yan, C.; Lin, Z.; Wu, J. Z.; Wang, J.; Yan, S. F.; Yan, N. The molecular basis of ABA-independent inhibition of PP2Cs by a subclass of PYL proteins. *Mol. Cell* **2011**, *42*, 662–672.
- (20) Santiago, J.; Dupeux, F.; Betz, K.; Antoni, R.; Gonzalez-Guzman, M.; Rodriguez, L.; Márquez, J. A.; Rodriguez, P. L. Structural insights into PYR/PYL/RCAR ABA receptors and PP2Cs. *Plant Sci.* **2012**, *182*, 3–11.
- (21) Wang, Z.; Ren, Z.; Cheng, C.; Wang, T.; Ji, H.; Zhao, Y.; Deng, Z.; Zhi, L.; Lu, J.; Wu, X.; Xu, S.; Cao, M.; Zhao, H.; Liu, L.; Zhu, J.; Li, X. Counteraction of ABA-Mediated Inhibition of Seed Germination and Seedling Establishment by ABA Signaling Terminator in Arabidopsis. *Mol. Plant* **2020**, *13*, 1284–1297.
- (22) Vaidya, A. S.; Peterson, F. C.; Eckhardt, J.; Xing, Z.; Park, S.-Y.; Dejonghe, W.; Takeuchi, J.; Pri-Tal, O.; Faria, J.; Elzinga, D.; Volkman, B. F.; Todoroki, Y.; Mosquna, A.; Okamoto, M.; Cutler, S. R. Click-tolead design of a picomolar ABA receptor antagonist with potent activity in vivo. *Proc. Natl. Acad. Sci. U. S. A.* **2021**, *118* (38), e2108281118.
- (23) Santiago, J.; Rodrigues, A.; Saez, A.; Rubio, S.; Antoni, R.; Dupeux, F.; Park, S.-Y.; Márquez, J. A.; Cutler, S. R.; Rodriguez, P. L. Modulation of drought resistance by the abscisic acid receptor PYL5 through inhibition of clade A PP2Cs. *Plant J.* **2009**, *60*, 575–588.
- (24) Pu, J.; Kentala, K.; Dickinson, B. C. Multidimensional Control of Cas9 by Evolved RNA Polymerase-Based Biosensors. *ACS Chem. Biol.* **2018**, *13*, 431–437.
- (25) Marguerat, S.; Schmidt, A.; Codlin, S.; Chen, W.; Aebersold, R.; Bähler, J. Quantitative analysis of fission yeast transcriptomes and proteomes in proliferating and quiescent cells. *Cell* **2012**, *151*, *671*–683.
- (26) Gómez-Schiavon, M.; Dods, G.; El-Samad, H.; Ng, A. H. Multidimensional Characterization of Parts Enhances Modeling Accuracy in Genetic Circuits. *ACS Synth. Biol.* **2020**, *9*, 2917–2926.
- (27) Dixon, A. S.; Schwinn, M. K.; Hall, M. P.; Zimmerman, K.; Otto, P.; Lubben, T. H.; Butler, B. L.; Binkowski, B. F.; Machleidt, T.; Kirkland, T. A.; Wood, M. G.; Eggers, C. T.; Encell, L. P.; Wood, K. V. NanoLuc Complementation Reporter Optimized for Accurate Measurement of Protein Interactions in Cells. *ACS Chem. Biol.* **2016**, *11*, 400–408.
- (28) Segall-Shapiro, T. H.; Meyer, A. J.; Ellington, A. D.; Sontag, E. D.; Voigt, C. A. A "resource allocator" for transcription based on a highly fragmented T7 RNA polymerase. *Mol. Syst. Biol.* **2014**, *10*, 742.
- (29) Jones, K. A.; Snodgrass, H. M.; Belsare, K.; Dickinson, B. C.; Lewis, J. C. Phage-Assisted Continuous Evolution and Selection of Enzymes for Chemical Synthesis. *ACS Cent Sci.* **2021**, *7*, 1581–1590.

- (30) Yuan, Y.; Miao, J. Agrochemical control of gene expression using evolved split RNA polymerase. *bioRxiv* **2022**, DOI: 10.1101/2021.05.03.442273.
- (31) B10NUMB3R5. Useful fundamental numbers in molecular biology. 2010

Recommended by ACS

Caged Activators of Artificial Allosteric Protein Biosensors

Selvakumar Edwardraja, Kirill Alexandrov, et al.

APRIL 27, 2020

ACS SYNTHETIC BIOLOGY

READ **C**

Toward in Silico Modeling of Dynamic Combinatorial Libraries

Iuri Casciuc, Jean-Marie Lehn, et al.

MAY 27, 2022

ACS CENTRAL SCIENCE

READ 🔀

Engineering Protein Switches for Rapid Diagnostic Tests

Hope Adamson and Lars J. C. Jeuken

OCTOBER 14, 2020

ACS SENSORS

READ **M**

Evolving Small-Molecule Biosensors with Improved Performance and Reprogrammed Ligand Preference Using OrthoRep

Alex A. Javanpour and Chang C. Liu

OCTOBER 01, 2021

ACS SYNTHETIC BIOLOGY

READ **E**

Get More Suggestions >